AIAA JOURNAL
Vol. 40, No. 8, August 2002

Open-Loop Hover Testing of a Smart Rotor Model

Nikhil A. Koratkar* and Inderjit Chopra†
University of Maryland, College Park, Maryland 20742

The development and open-loop hover testing of a smart rotor model with trailing-edge flaps for individual blade control of helicopter vibration are presented. First, the University of Maryland Advanced Rotorcraft Code was used to size the trailing-edge flap and to determine the flap-deflection requirements for vibration suppression in the wind tunnel. Next an analytic model for the coupled actuator-flap-rotor system was used to develop a multilayer piezoelectric bender configuration that was capable of meeting the flap-deflection requirements. Based on this study, a matched set of six smart rotor blades were fabricated in-house. The four-bladed smart rotor model was tested in the open-loop mode in hover using a Bell-412 Mach-scaled hub. Flap deflections of ±4 to ±6 deg were recorded in the 1–5/rev frequency range at the model operating speed of 1800 rpm. The flap deflection increased to ±23 deg at 8/rev because of actuator resonant amplification. Rotor collective pitch was found to have negligible impact on actuator performance. The maximum control effectiveness was observed close to the blade flatwise bending and torsion natural frequencies. For 3/rev actuator excitation oscillatory thrust levels of up to ±10 lb (45 N) (60% steady rotor blade thrust at 6-deg collective) were recorded, thereby demonstrating the open-loop control authority of the actuator-flap system.

I. Introduction

THE helicopter spends a large portion of its operation in forward flight, resulting in an aerodynamic asymmetry between the advancing and retreating sides of the rotor disk. As a result of this, the rotor flowfield is extremely complex and can include transonic flow on the advancing blade tip, dynamic stall on the retreating side of the disk, highly yawed and reversed flows, and blade-wake interactions with tip vortices from preceding blades. This highly complex and nonsteady aerodynamic environment and the dynamic response of the long and flexible rotor blades result in large vibratory forces, which are filtered through the hub to the fuselage. Typically for an N-bladed rotor, the dominant $N-1$, N and $N+1$/rev blade loads are transmitted to the fuselage as an N/rev forcing.

Reduction in vibration and noise levels of the helicopter yield benefits in terms of improved passenger comfort, reduced crew fatigue, improved community acceptance, and increased fatigue life of structural components. Currently, passive isolators and absorbers are routinely used to reduce vibration. However these devices cause significant weight penalties (up to 3% of gross weight) and rapidly degrade in performance away from the tuned flight condition. In contrast, active vibration reduction schemes offer the promise of achieving reliable vibration reduction over a wide range of operating conditions with lower weight penalty than conventional passive methods.

There are two types of rotating frame active control systems: higher harmonic control (HHC) and individual blade control (IBC). HHC involves excitation of the swashplate at N/rev. The major disadvantage of HHC is the high actuation power required to pitch the rotor blades particularly in extreme flight conditions and large weight penalties associated with the hydraulic actuators. Another important limitation is that HHC is limited to N/rev excitation of the swashplate. However, for performance improvement, dynamic stall alleviation, acoustic control, and alleviation of gusts and maneuvering loads more broadband actuation is necessary. The search for a solution to these limitations resulted in the development of the concept of IBC.

IBC involves generation of unsteady airloads by excitation of each blade independent of the others. This eliminates the frequency restriction of HHC because the individual blade can be excited in the time domain with any desired input waveform. Conventional IBC involves blade-root pitch excitation using hydraulic actuators that are mounted in conjunction with the pitch-links. Wind-tunnel testing[1] and flight-test evaluation[2] of an IBC system was carried out on the Eurocopter B0-105. These tests showed that significant reductions in vibration and noise levels were attainable. The complexity and weight of the hydraulic slip ring unit is the primary reason why the concept of IBC, which has enormous potential, has not been able to make the transition toward practical implementation on commercial helicopter systems. Another important drawback is that conventional IBC requires the dynamic pitching of the entire rotor blade up to frequencies of $N+1$/rev, leading to large actuation power requirements. The key to solving the just-mentioned technical challenges could lie in the concept of on-blade actuation using smart materials. Straub and Merkley[3] showed that using on-blade all moving aerodynamic control surfaces like trailing-edge flaps can significantly reduce actuation power requirements for IBC. Also, the use of smart material driven actuation systems significantly reduces actuation power and weight penalty and eliminates the need for a heavy, cumbersome, and complex hydraulic slip ring in favor of a much simpler electrical slip ring. Thus on-blade actuation using smart materials has the potential to revolutionize IBC technology.

The present authors[4] designed and tested a Froude-scaled rotor model with on-blade actuation using smart materials. A four-layered piezoelectric bender was used to drive a 4% span, 20% chord flap located at 95% spanwise location. Flap deflections of ±6 deg at 4/rev were achieved in hover at the Froude-scaled operating speed of 900 rpm. At NASA Ames Research Center, Moffett Field, California, Fulton and Ormiston[5] have conducted wind-tunnel tests on a Froude-scaled rotor model with piezo-bender actuation. The tests successfully demonstrated the effectiveness of on-blade elevon controls for significantly reducing or cancelling individual 3, 4, and 5/rev harmonic blade vibratory flap bending moments. Various alternatives to piezoelectric bender actuation have also emerged. Prechtl and Hall[6] have proposed a piezoelectric stack based actuation mechanism (X-frame) for on-blade actuation of a trailing-edge flap. The actuator was integrated into a $\frac{1}{6}$th Mach-scale Boeing CH-47 (Chinook) blade with an 11.5% span and 20% chord flap and tested in hover. At the operating speed (tip Mach number 0.63) and 8-deg collective, flap

Received 13 February 2001; revision received 7 February 2002; accepted for publication 13 February 2002.

*Graduate Research Assistant, Alfred Gessow Rotorcraft Center, Department of Aerospace Engineering; currently Assistant Professor, Department of Mechanical, Aerospace and Nuclear Engineering, Rensselaer Polytechnic Institute, 110 8th Street, Troy, NY 12180.

†Professor and Director, Alfred Gessow Rotorcraft Center, Department of Aerospace Engineering. Fellow AIAA.

deflections of ±2.4 deg were achieved. At the University of Maryland, Lee and Chopra[7] have designed a bidirectional piezostack actuator incorporating a double-lever stroke amplifier. At Pennsylvania State University, Centrolonza and Smith[8] has proposed a shear mode piezoelectric torque tube as a candidate for a full-scale flap actuator. In another study Fink[9] has used a proprietary electromagnetic actuator to drive an 11.3% span, 46% chord flap on the OH-58 (Kiowa Warrior) rotor blade. Flap deflections of ±6 deg were recorded at a tip Mach number of 0.48 (81% design value) in hover. A major drawback of this actuator is very high power consumption (up to 4 kW) away from the actuator resonance condition. In another study Bernhard and Chopra[10] proposed a smart active blade tip for vibration control. The active tip (with 10% span) was driven by a novel piezo-induced bending-torsion coupled actuator beam, located spanwise in the hollow midcell of the main rotor blade. In hover at 2000 rpm (tip Mach number 0.5) active tip deflections of over ±5 deg were achieved with over 50% variation in the steady rotor thrust levels at 8-deg collective.

Active twist rotors involving direct torsional actuation of the rotor blade have also been proposed as an alternative to rotors with trailing-edge flaps. Chen and Chopra[11] developed a Froude-scaled active twist rotor featuring banks of specially shaped monolithic piezoelectric elements. At reduced tip speed (0.24 Mach number) tip twist amplitudes of ±0.4 deg were demonstrated with associated oscillatory thrust perturbations of up to 10% of steady rotor thrust at 8-deg collective. Recent years have seen enormous advancements in active twist rotor technology with the development of active fiber composites (AFC) along with interdigitated electrodes to activate the piezofibers in the d-33 mode. Rodgers and Hagood[12] tested a two-bladed $\frac{1}{6}$th Mach-scale model of the Boeing CH-47 Chinook rotor with AFC technology. Tip twist amplitudes of ±0.4 deg were demonstrated at full rotor speed (0.63 Mach number) and 8-deg collective. Subsequently, Wilbur et al.[13] and his associates have tested a $\frac{1}{6}$ model in heavy gas medium at the NASA Langley transonic wind tunnel. During open-loop tests, oscillatory tip twist amplitudes of up to ±1 deg were recorded in the 3–5/rev frequency range.

A review of the state of the art shows that the focus of small-scale smart rotor research has shifted from the development of Froude-scaled models toward the development of Mach-scaled prototypes[12–14] that are more representative of full-scale flight conditions. However most of the research has been restricted to open-loop tests on the hover stand. Therefore, there is a need to couple the smart rotor model with a controller and demonstrate vibration reduction by conducting closed-loop vibration control tests in the wind tunnel. It is hoped that such realistic tests involving smart rotor blades will provide valuable physical insight into the behavior of the coupled actuator-flap-rotor system. The present research is focused toward conducting a full four-bladed closed-loop vibration suppression test in the wind tunnel. However, prior to closed-loop testing, it becomes necessary to characterize the open-loop actuator-flap-rotor system dynamics. The present paper will cover open-loop actuator voltage and frequency sweep tests conducted at different rotor speeds and collective pitch settings. These tests are conducted on the hover test stand at the University of Maryland. The objective of these tests is to characterize the system dynamics and to demonstrate the open-loop control authority of the actuator-flap system.

II. Actuation Mechanism

The bender used in this study consists of PZT-5H (lead–zirconate–titanate) piezoceramic sheets that are bonded to a very thin brass shim with an electrically conductive adhesive coating. The bender is cantilevered, and PZT sheets on opposite sides of the shim are excited out of phase. Therefore, if the PZT sheets on one side of the shim are in extension, the PZT sheets on the other side of the shim will be in compression and vice versa. This causes a pure bending of the actuator, and the resulting tip displacement provides the actuation mechanism for the flap. The tip displacement of the bender is very small (10 mils; 0.0254 cm) and must be amplified using a mechanical leverage mechanism (Fig. 1). To adapt the bender with the linkage used for connection to the flap, a rod was molded onto the bender tip using E-glass cloth. This rod fits inside a tiny machined cusp. The cusp is an integral part of the flap. As the bender moves up and down, the molded tip moves slightly in and out of the cusp and rotates the flap. In the present design the distance between the flap hinge and bender-cusp contact point acts as the effective lever arm length.

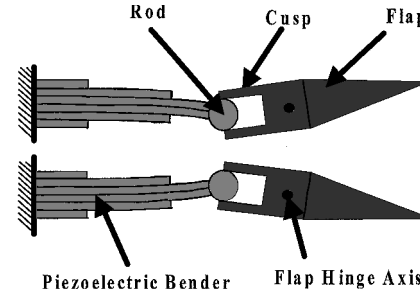

Fig. 1 Piezoelectric bender actuation mechanism.

III. Smart Rotor Model Development

This section will describe the development of the smart rotor system. First the model operating conditions are discussed, and then the University of Maryland Advanced Rotorcraft Code (UMARC) is used to determine the optimum trailing-edge flap sizing and location as well as the deflection requirements for vibration reduction in the wind tunnel. Next, an in-house rotor code for the coupled actuator-flap-rotor system is used to determine a piezoelectric bender configuration that is capable of achieving the desired flap-deflection amplitudes. Based on this study, a matched set of six smart rotor blades were fabricated in house.

A. Rotor Geometry and Model Operating Conditions

The rotor radius, chord, and external geometry are determined by the available rotor mold used for blade fabrication. The rotor diameter is 5 ft (1.52 m), chord is 3 in. (7.62 cm), and the airfoil section has a NACA 0012 profile. The blades have a rectangular planform and zero twist. The symmetric profile, zero twist, and rectangular planform greatly simplify the fabrication at the expense of rotor performance (figure of merit and maximum thrust). The present research is focused on developing a technology demonstrator for active vibration control, with baseline rotor performance characteristics being of secondary importance. Consequently, the untwisted, rectangular planform rotor with NACA 0012 airfoil section is adequate to address the issue of actuator-flap control authority in the rotating environment. The rotor blade dimensions and structural mass and stiffness properties are listed in Table 1.

The active rotor is to be tested using a Bell-412 Mach-scaled bearingless rotor hub. The flexbeams of the Bell-412 hub are rated for a maximum tensile load of 1200 lb (5341 N). As shown in Table 1, the smart rotor blade mass is 284 g. This translates to a maximum safe operating rpm of 1840 (without exceeding the centrifugal load limits of the flexbeam). A rotor speed of 1800 rpm was selected for the present model to give additional safety margin. At 1800 rpm the hover tip Mach number is 0.45. This is about 20–30% lower than typical full-scale hover tip Mach numbers that are in the range from 0.6 to 0.65. The Lock number of the present model is 3.4. This is also lower than typical full-scale Lock numbers[10] that are in the range from 4 to 7. The low Lock number is an indication of the larger mass of the present rotor blade (284 g) as compared to the Bell-412 baseline rotor (196 g). The Reynolds number of the smart rotor model is $\frac{1}{7}$th the full-scale value. Despite these limitations, small-scale models are indispensable for low-cost, low-risk, proof-of-concept validation and controller development.

B. Flap Parametric Study

To achieve vibration reduction for the smart rotor, it is necessary to determine the optimal flap location and sizing for minimal actuation power requirements. The flap parametric study was conducted using UMARC. The details regarding UMARC and the flap parametric study are available in Ref. 14. The flap design optimization study[14] converged to an 8% span, 20% chord, and trailing-edge flap located at 75% rotor radius. For this configuration the required peak-to-peak

Table 1 Smart rotor blade properties

Property	Dimension
Rotor diameter	5 ft (1.52 m)
Blade chord	3 in. (7.62 cm)
Blade twist	0 deg
Blade planform	Rectangular (no taper)
Airfoil section	NACA 0012
Operating speed	1800 rpm
Tip Mach number	0.45
Froude number	2760 g
Lock number	3.4
Trailing-edge flap span	2.4 in. (6.07 cm) (8% span)
Trailing-edge flap chord	0.6 in. (1.524 cm) (20% chord)
Trailing-edge flap radial location	75% span
Actuator	Eight-layered, tapered bender
Actuation system mass	47 g
Rotor-blade mass	284 g
Blade section flat-wise bending stiffness	6771.7 lb · in.^{2} (19.43 N · m^2)
Blade section torsion stiffness	2298.2 lb · in.^{2} (6.59 N · m^2)
Sectional center of gravity	26% chord
Sectional elastic axis	23.5% chord
Blade first torsion frequency	3.1/rev at 1800 rpm
Actuator first flat-wise bending frequency	8/rev at 1800 rpm

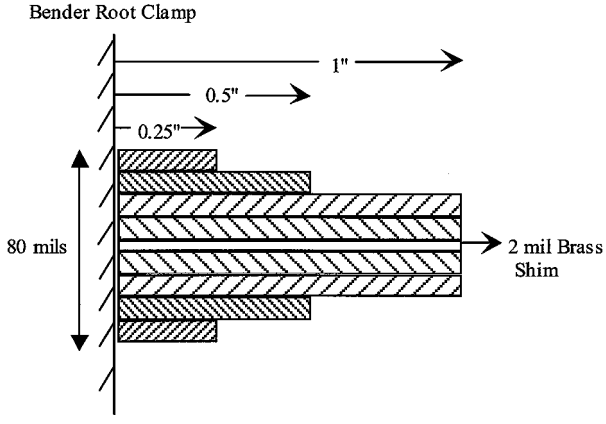

Fig. 2 Eight-layered, tapered piezoelectric bender.

flap deflection for over 95% reduction in the vibration index is 8-deg peak-peak (±4-deg amplitude). The vibration index J is expressed as

$$J = y^T W_y y \tag{1}$$

where W_y is the weighting matrix for the vibratory loads and y represents the vibratory hub loads in the fixed frame. Equal weighting was given in this study to all six vibratory hub loads, and no trailing-edge flap effectiveness factors were used.

C. Actuator Design

The goal of the actuation system is to deflect an 8% span, 20% chord flap located at 75% rotor radius by ±4 deg. The conventional piezoelectric bimorph consists of a piezoceramic sheet bonded to the top and bottom surface of a brass shim. By bonding additional layers on both sides of the shim, it is possible to construct multilayered piezoactuators. Increasing the number of PZT layers results in greater actuation force capability for the piezobender at the cost of reduced stroke. By tapering the bender, the piezoinduced bending and the actuator stiffness are optimized, resulting in improved force-stroke characteristics.[14,15] For the present smart rotor model an eight-layered tapered piezobender (Fig. 2) was selected for actuating the trailing-edge flap. Additionally an ac bias circuit[15] was used to extend the depolarization limit and apply higher input voltages to the eight-layered actuator.

D. Predicted Flap Deflections

For the present rotor system the actuator is coupled to the rotor response and vice versa. Therefore, it becomes necessary to integrate the actuator model into the rotor analysis. In Ref. 15 the authors presented an analytic model for the coupled actuator-flap-rotor dynamic response in hover. This model is used to predict actuator-flap performance in the rotating environment. The analysis indicated that for a 180 Vrms excitation the eight-layered tapered actuator is able to deflect the 8% span and 20% chord flap located at 75% rotor radius by the required ±4 deg in the 1–5/rev frequency range (30–150 Hz) at 1800 rpm in hover.

E. Rotor-Blade Fabrication

Having selected the actuator and trailing-edge flap design parameters, the next step is rotor blade fabrication and system integration. Figure 3a is a schematic of the smart rotor-blade layout. The primary load carrying member is a graphite-epoxy composite spar that is designed to carry a tensile force of 3800 lb (16,914 N) (factor of safety of 3). The composite spar has a $[0/+45/-45/90]_s$ layup and a rectangular cross section with dimensions of 0.269 × 0.053 in. (0.68 × 0.13 cm). The spar is bolted on to an aluminum root insert, which is precision machined to match the NACA 0012 airfoil contour. Tantalum leading-edge weights are used to mass balance the blade. These leading-edge weights are embedded in specially designed rib cages (Fig. 3a), which are in turn bonded to the spar using a high-strength film adhesive. The anchor plate, which supports the actuator-flap mechanism, is also bonded to the spar using the film adhesive.

This skeletal assembly is then embedded in a Rohacell IG-71 foam core, and three plies of 5-mil (0.0127-cm)-thick, [0, 90] prepreg E-glass cloth are wrapped over the foam. The top and bottom surfaces of the spar get bonded to the skin as it wraps around the foam core resulting in a two-celled cross section. The foam core along with the skin is cured in the rotor mold. The actuator is accessed via a removable panel that covers the actuator and anchor plate assembly. The trailing-edge flap is fabricated separately using rohacell foam and a single 5-mil (0.0127-cm) prepreg E-glass skin. The trailing-edge flap motion is measured in the rotating frame using a Hall-effect sensor. Figure 3b shows the finished rotor blade and rotor mold used for blade fabrication. The mass of the smart rotor blade is 284 g, whereas the mass of the actuation system (actuator, anchor plate, clamp plates, leading-edge weights for mass balancing, etc.) is about 47 g (24% of baseline Bell-412 blade mass). Table 1 summarizes the important parameters of the active rotor system.

F. Thrust-Bearing Design

For the present model the centrifugal acceleration at the blade tip is 2760 g at 1800 rpm. This large centrifugal acceleration results in very severe frictional losses associated with the trailing-edge flap hinge mechanism. To minimize the frictional losses, it becomes necessary to mount a dedicated thrust bearing to support the trailing-edge flap in the radial direction. At the present scale size limitations preclude the use of a conventional roller thrust bearing; consequently, a microthrust ball bearing[16] was selected. The F2-6 bearing has a bore diameter of 2 mm, outside diameter of 6 mm, static load capacity of 19.39 lb (86.3 N), and dynamic load capacity of 26.44 lb (117.6 N). For ideal operation the F2-6 bearing should provide a coefficient of friction of 0.05.

IV. Active Rotor Fan Plot

The fan plot shows the placement of rotor blade and actuator natural frequencies with respect to the rotor harmonics. For a conventional passive rotor the flap-bending, lag-bending, and torsional natural frequencies are separated from the rotor harmonics in order to minimize the baseline vibration levels and improve the fatigue life of the blades. Conventional swashplate-based rotor systems are typically designed as stiff in torsion in order to ensure aeroelastic stability. On the other hand, helicopters that use servoflaps for primary rotor control are designed as soft in torsion, in order to enhance servoflap control effectiveness.

The fan diagram (Fig. 4) for the present rotor model was generated using the analytic model developed in Ref. 15. The actuator first flat-wise bending natural frequency increases from 190 Hz at 0 rpm to 240 Hz (8/rev) at 1800 rpm as a result of aerodynamic and centrifugal stiffening of the actuator beam. Thus the resonance of the actuator is at 8/rev (240 Hz), which indicates that the actuator has sufficient bandwidth for operation in the 3–5/rev (90–150-Hz)

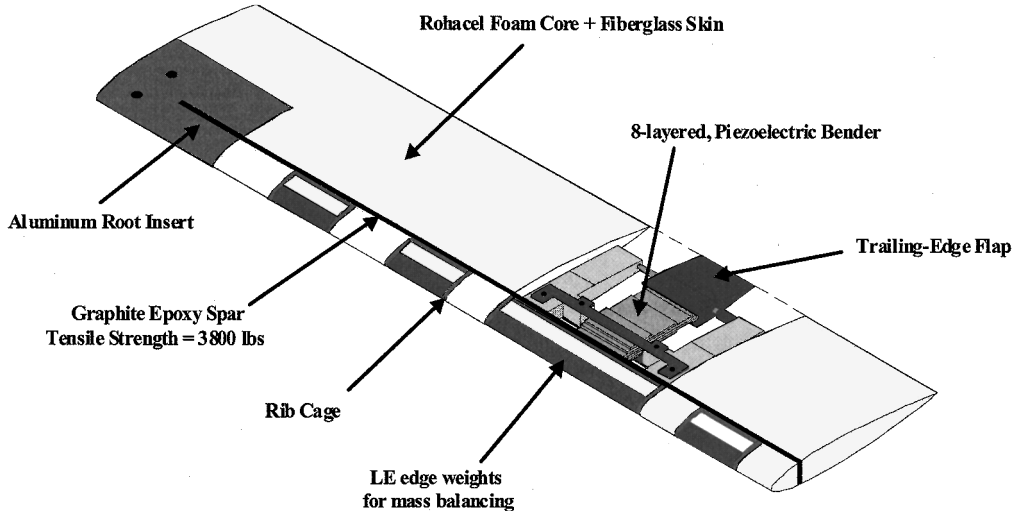

a) Smart rotor model layout

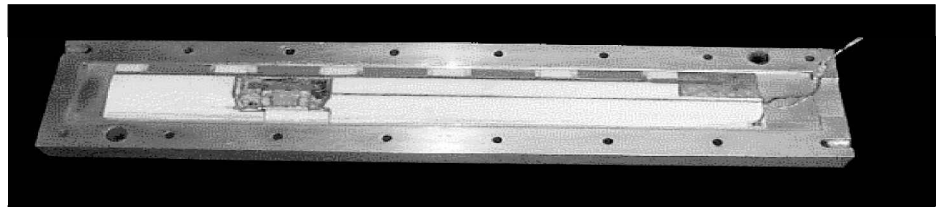

b) Finished rotor blade with rotor mold

Fig. 3 Smart rotor-blade fabrication.

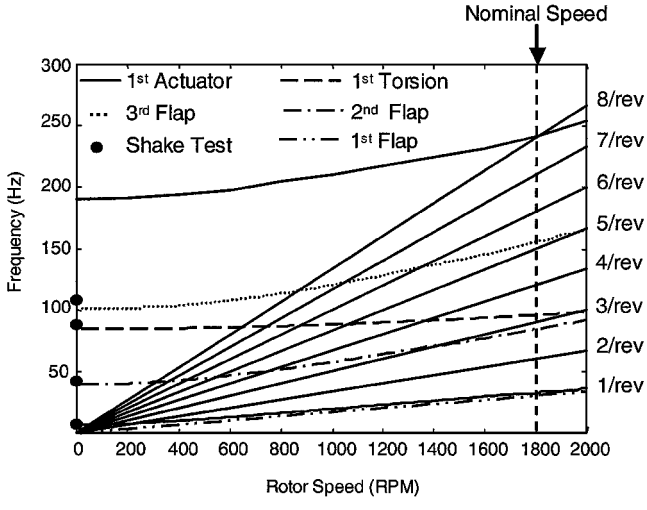

Fig. 4 Fan diagram for smart rotor model in air at 2-deg collective pitch.

frequency range. The smart rotor is four bladed, and hence the vibration reduction capability of the actuator-flap system depends primarily on the control authority at 3, 4, and 5/rev excitation frequencies. Hence the blade first torsion natural frequency (3.1/rev at 1800 rpm) and third flat-wise bending natural frequency (5.13/rev at 1800 rpm) have been placed close to the 3/rev and 5/rev rotor harmonics (as shown in Fig. 4) in order to maximize actuator-flap control authority in the 3–5/rev frequency range.

V. Hover Testing

This section will describe the open-loop testing of the smart rotor model on the University of Maryland hover test stand. The test stand is a 12-ft (3.65-m) tower providing in excess of two rotor diameters ground and ceiling clearance. The rotor shaft is driven by a 2:1 reduction belt drive from a hydraulic motor. A Bell-412 Mach-scaled bearingless rotor hub[17] is mounted on the hover test stand. This hub consists of two composite yokes that are stacked perpendicular to each other. One blade is mounted at one end of each yoke, resulting in a four-bladed rotor system. The yokes are designed to act as virtual hinges for blade flat-wise and lag-wise bending. Blade feathering is achieved via elastomeric pitch bearings. Elastomeric lag dampers are also mounted on the flexbeams to ensure aeroelastic stability. Figure 5 shows a photograph of the rotor test rig along with two smart rotor blades. Data transfer between the rotating and fixed frames was carried out using two independent slip rings, one for actuation and the other for sensing purposes. The physical decoupling of the actuation and sensing lines minimizes the possibility of cross talk between the power and signal lines. The data acquisition system consisted of a National Instruments board (PCI-6071E) with 32 differential input channels running on dual Pentium-3, 600-MHz processors. This system was used for performing single-frequency dwell tests. Additionally, frequency sweep (swept sine) tests were also conducted using a Siglab model 20-42 digital signal processing system.[18] The amplifiers used to drive the eight-layered tapered piezoelectric benders are PA 9810 precision power amplifiers developed by Rohrer Systemtechnik.[19]

Prior to spin testing, the blades were statically balanced. The four smart rotor blades were balanced to within ±2 g (0.67% of blade weight) and a radial center of gravity within ±0.1 in. (0.254 cm) (0.33% rotor radius). Nonrotating shake tests were also conducted to measure the nonrotating blade frequencies. Figure 4 compares the experimentally measured blade flap and torsion frequencies with the predictions. The analytic model developed in Ref. 15 shows good agreement with test data for the nonrotating natural frequencies. Next, the rotor speed was increased to 1500 rpm and then to 1800 rpm checking rotor track and balance at both speeds. Four types of open-loop tests were conducted: rpm sweep tests, voltage sweep tests, frequency sweep tests, and collective sweep tests. For all of the preceding tests, the actuator current and power consumption were also recorded and compared with predictions. For this study only one blade was activated at a time. Up to 20% variation in the flap-deflection response of individual blades was observed as a result of differences in actuator characteristics as well as thrust bearing alignment and assembly.

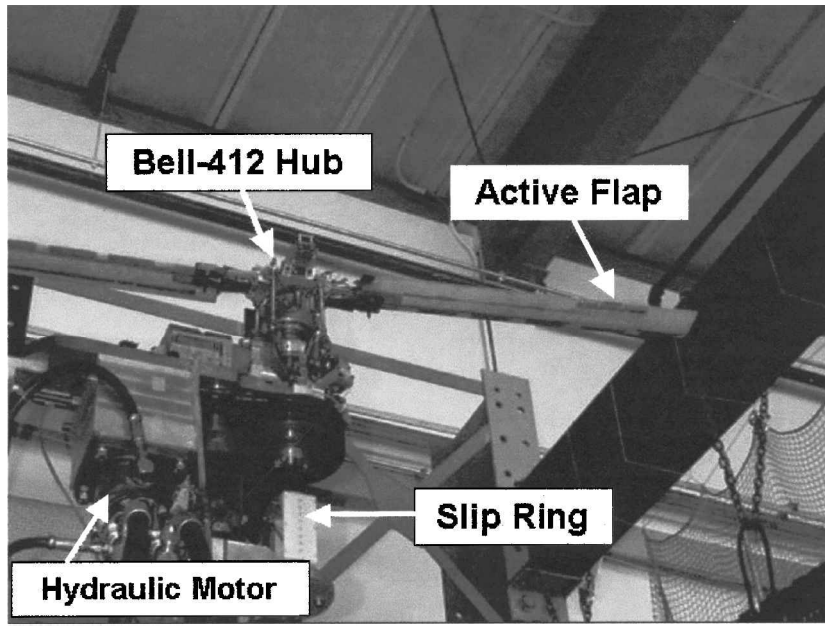

Fig. 5 Hover stand test facility.

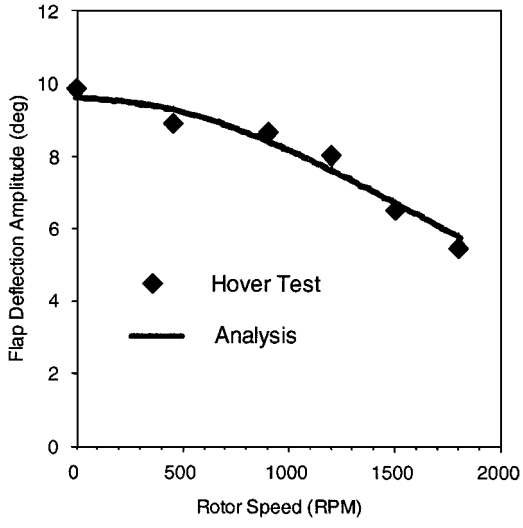

Fig. 6 Hover test: rpm sweep (input, 180 Vrms at 10 Hz and collective, 2 deg).

A. RPM Sweep Test

The objective of this test is to quantify the influence of rotor speed on actuator performance in the rotating environment. The rotor speed is increased to the nominal operating speed of 1800 rpm, and the actuator on blade 1 is excited at 180 Vrms and 10 Hz. The rotor collective pitch is set at 2 deg. Figure 6 shows the trailing-edge flap-deflection response at different rotor speeds measured using the Hall-effect sensor for blade 1. The flap-deflection response degrades from ±10 deg (nonrotating capability) to ±5.5 deg at 1800 rpm. Analytic predictions show good correlation with the hover test data.

The nearly 50% degradation in actuator performance shown in Fig. 6 is caused by the trailing-edge flap hinge moment, which opposes the piezoinduced bending of the actuator beam. A detailed description of the individual contributions to the trailing-edge flap hinge moments are provided in Ref. 15. The frictional hinge moment associated with the thrust bearing accounts for nearly 50% of the degradation in actuator performance. The aerodynamic hinge moment accounts for about 40% of the decay, whereas the propeller and inertial hinge moments are responsible for the remaining 10%. In spite of these losses, the actuator has sufficient authority to meet the design deflection requirements of ±4 deg at 1800 rpm.

The aerodynamic hinge moment can be reduced by aerodynamic balancing of the trailing-edge flap (that is, designing the flap as an airfoil section with the hinge axis located at its quarter-chord); however, redesign of the rod-cusp stroke amplifier is necessary to connect the aerodynamically balanced flap to the actuator beam. The frictional hinge moment depends primarily on the mass of the flap, coefficient of friction at blade-flap interface, and centrifugal acceleration (g loading). The trailing-edge flaps used on the present model were optimized with a view to mass reduction. Consequently, the trailing-edge flap mass is only 3.1 g (1% rotor blade mass), and no further reduction appears feasible. Because of the installation of the thrust bearing to support the flap, the coefficient of friction was also minimized. In Ref. 15 the authors conducted a vacuum chamber spin test and showed that the coefficient of friction at the blade-flap interface was as low as 0.05. Thus the only possibility of further reduction in the frictional hinge moment is to test the model in heavy gas medium, which allows for Mach scaling at lower centrifugal accelerations (about 800 g). Thus there is some opportunity for improvement in actuator performance; however, Fig. 6 indicates that even in the present configuration the actuator is able to achieve the design target of ±4 deg at 1800 rpm.

B. Voltage Sweep Test

The objective of this test is to quantify the influence of the amplitude of the excitation voltage on actuator performance. For the present test the rotor speed is held constant at 1500 rpm, and the collective pitch is 2 deg. The actuator on blade 2 is excited at four different excitation voltages, 180, 130, 100, and 50 Vrms, and at excitation frequencies ranging from 1/rev (25 Hz) to 5/rev (125 Hz). Figure 7 compares the measured trailing-edge flap deflections with analytic predictions. There is good agreement between the analysis and hover test data.

Figure 7 indicates that the flap-deflection amplitude at 180 Vrms and 1/rev (±6 deg) is about 20 times the flap-deflection amplitude at 50 Vrms and 1/rev (±0.3 deg). Thus the improvement in actuator performance with increase in excitation voltage is nonlinear, and this is a reflection of the nonlinearity of the PZT induced strain response with respect to the applied electric field.[20] Increasing the applied voltage above 200 Vrms is not recommended because of the possibility of PZT arcing and/or dielectric breakdown.

C. Collective Sweep Test

The objective of the present test is to study the influence of rotor-blade collective pitch on actuator performance. The rotor collective pitch affects the rotor steady loads, inflow and coning angle, and is an important control input for vehicle trim in both hover as well as forward flight. The smart rotor model is tested at 2-, 4-, and 6-deg collective. For each collective setting the rotor speed is held constant

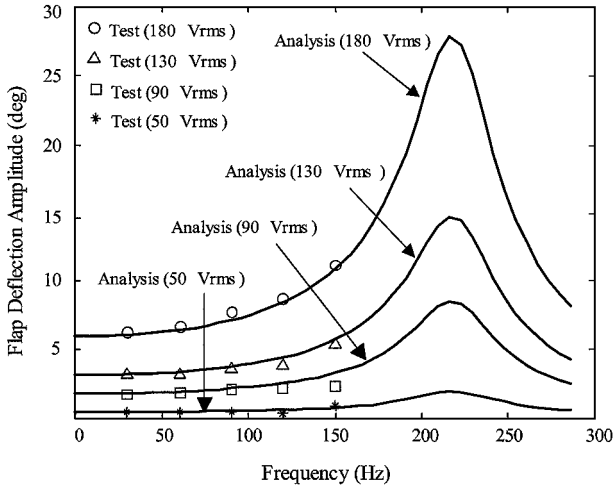

Fig. 7 Hover test: voltage sweep (rotor speed, 1500 rpm and collective pitch, 2 deg).

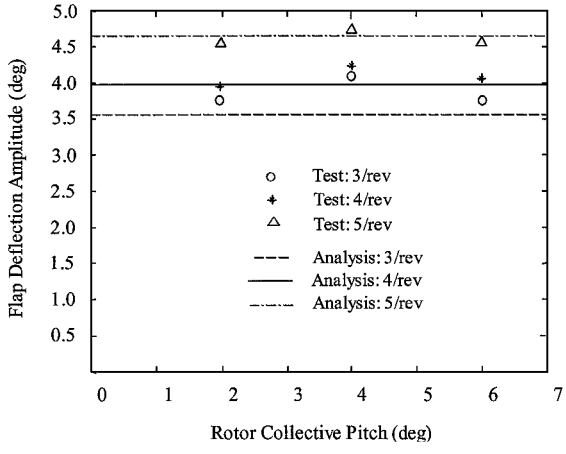

Fig. 8 Hover test: collective sweep (input, 150 Vrms; excitation frequencies, 3, 4, and 5/rev; and rotor speed, 1800 rpm).

at 1800 rpm. At 6-deg collective and 1800 rpm the nondimensional rotor thrust coefficient C_T for the rotor model is 0.005.

At each collective setting the actuator on blade 3 was excited at 150 Vrms at frequencies of 3, 4, and 5/rev. Figure 8 shows the influence of collective pitch on flap-deflection response. No significant degradation in actuator performance is observed with collective pitch variation. Therefore, blade steady loads are found to have negligible impact on the actuator-flap dynamic response. This implies that the vehicle trim settings such as collective and cyclic pitch inputs are expected to have a small influence on the vibration suppression capability of the actuator-flap system.

D. Frequency Sweep Tests

Frequency sweep tests are conducted to establish the influence of excitation frequency on actuator-flap control authority. For these tests a Siglab 20-42 digital signal processing system[18] is used to conduct an actuator sine sweep test from 5 to 185 Hz (0.16 to 6.16/rev). All frequency sweeps are conducted with 1.5-Hz frequency steps, 3 averages, and a tracking filter bandwidth of 2 Hz. The output of the sine sweep test yields the transfer function between the voltage input and the trailing-edge flap deflections and associated oscillatory rotor hub loads. For all of the tests presented in this section, only one blade (blade 4) is activated.

1. *Flap-Deflection Response*

Figure 9a shows the trailing-edge flap-deflection transfer function at 1800 rpm. The rotor collective pitch is 2 deg, and actuator excitation voltage is 180 Vrms. There is good agreement between the test data and predictions. The analysis correctly predicts the actuator-flap natural frequency as 240 Hz (8/rev). In the 3–5/rev

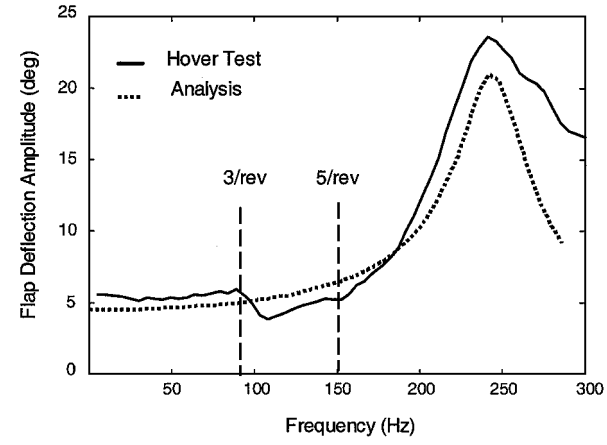

a) Trailing-edge flap deflection response

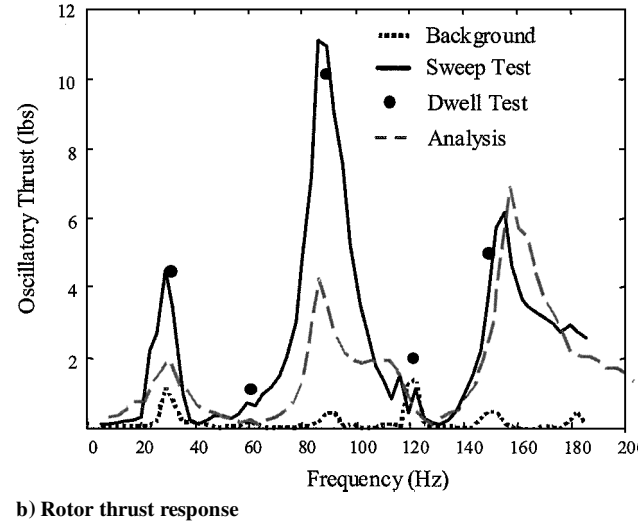

b) Rotor thrust response

Fig. 9 Hover test: frequency sweep (input, 180 Vrms; rotor speed, 1800 rpm; and collective pitch, 2 deg).

range (90–150 Hz) no resonant amplification is observed, and the flap response (±4.5 deg) is fairly uniform. However, at 240 Hz (8/rev) flap-deflection amplitudes of over ±23 deg were recorded because of actuator resonant amplification. Operating in the vicinity of the resonant amplification peak for a prolonged duration is not recommended because the large induced strain levels can cause actuator overheating and depolarization leading to severe reduction in actuator fatigue life. Additionally, sharp phase roll-off in the proximity of the resonant frequency increases the complexity of the control system design for active vibration suppression. For these reasons the actuator mass and stiffness distribution have been tailored to ensure sufficient margin between the resonant frequency (8/rev) and the operating range (3 to 5/rev) of the actuator.

2. *Rotor Thrust Response*

Figure 9b shows the oscillatory rotor thrust levels with and without actuator excitation for a sine sweep test conducted at 1800 rpm and 2-deg collective. The thrust signal is measured using a six-component fixed frame balance connected to the base of the rotor shaft. The balance was dynamically calibrated[21] to measure fixed frame hub forces and moments. Figure 9b shows that the actuator-flap open-loop control authority is highly frequency dependent. The thrust authority shows a dramatic increase when the excitation frequency is close to the blade flat-wise bending and torsion natural frequencies. Large actuator-flap control effectiveness is observed close to the first flat-wise bending frequency (31.8 Hz: 1.06/rev), first torsion frequency (93 Hz: 3.1/rev), and third flat-wise bending frequency (154 Hz: 5.13/rev). The analytic model developed in Ref. 15 is able to predict these trends. The large oscillatory thrust induced by the trailing-edge flap actuation close to the blade structural modes is a reflection of the low Lock number of the present

rotor model, which manifests itself in the form of reduced aerodynamic damping levels. The trailing-edge flap does not excite the blade second flat-wise bending mode because the midsection of the trailing-edge flap is located at 75% rotor radius, which corresponds to the node of the second flat-wise bending mode.

For vibration control the trailing-edge flap is required to be excited at the rotor harmonics (example: 3, 4, and 5/rev for a four-bladed rotor). To verify the accuracy of the sine-sweep tests, single-frequency dwell tests are also performed at the rotor harmonics. The actuator is excited at 180 Vrms at frequencies of 1, 2, 3, 4, and 5/rev. Figure 9b shows that the sine sweep tests and single-frequency dwell tests show good agreement. For a 3/rev actuator excitation the oscillatory rotor thrust amplitude is ±10.2 lb (45 N) (thrust coefficient: ±0.001), which corresponds to 60% variation in the steady thrust per blade at 6-deg collective pitch.

For the present smart rotor model the first torsion and third flat-wise bending natural frequencies have been placed close to the 3/rev and 5/rev harmonics (see fan plot, Fig. 4) in order to maximize actuator-flap control authority in the 3–5/rev frequency range. The preceding design approach is quite contrary to conventional passive rotor-blade design. For conventional rotors the blade structural frequencies are placed as far away as possible from the rotor harmonics in order to reduce the baseline vibration levels and maximize blade fatigue life. However, the present study (Fig. 9b) indicates that retrofitting a trailing-edge flap on to an existing rotor blade will not yield the optimum system in terms of actuator control effort. To minimize actuator requirements, the rotor blade must be considered as part of the active unit, and the placement of rotor blade structural frequencies must be carried out with a view to minimizing actuator control effort. At the same time it has to be borne in mind that changing the rotor-blade frequency placement will alter the background (uncontrolled) vibration levels and this will also affect the actuator requirements.

E. Actuator Current and Power

An important aspect of actuator performance is the actuator current and power consumption. The current is a useful parameter to monitor the health of the piezoceramic elements, particularly in terms of piezocracking and overheating. In Ref. 20 Sirohi and Chopra modeled the piezoceramic elements as lossy capacitors, with electric-field-dependent capacitance and loss factor. This approach will be used in the present study to predict actuator current and power consumption.

The smart rotor model is tested at 1800 rpm and 6-deg collective. Single-frequency dwell tests are conducted at the first five rotor harmonics (1 to 5/rev), and the actuator is excited at four different excitation voltages, namely, 50, 100, 130, and 180 Vrms. Figure 10 shows the measured actuator current for different voltage settings and excitation frequencies for blade 1 along with predictions. The

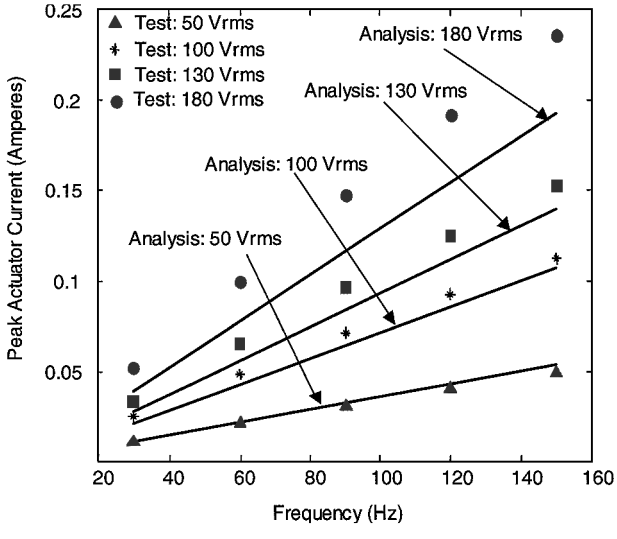

Fig. 10 Hover test: actuator current consumption (rotor speed, 1800 rpm and collective pitch, 6 deg).

current required by the actuator increases with the amplitude of the voltage signal and frequency of excitation. The analysis shows good agreement for 50- and 100-Vrms inputs. However for 130- and 180-Vrms excitation the analysis underpredicts the test data, particularly at higher frequencies. There are two probable causes for this discrepancy. First, piezoceramics and PZT-5H in particular exhibit strong variation in permittivity[20] with temperature. Hence self-heating of the PZT results in higher permittivity and consequently higher current. As the amplitude and frequency of the applied signal increases, PZT self-heating[20] effects become more prominent, resulting in higher measured current. Second, the empirical constants used to model the nonlinear electric field dependent permittivity are strictly valid only up to 4.5×10^5 Vrms/mil (1.77×10^8 Vrms/cm). For the PZT-5H sheets used on the bender, at 180 Vrms the electric field is 11.81×10^5 Vrms/mil (4.64×10^8 Vrms/cm). Thus the electric field far exceeds the valid range for the empirical constants, and hence the analysis for the 130- and 180-Vrms cases has to be considered with uncertainty bounds.

Figure 10 shows that the maximum current consumption is 0.2278 A (peak), which corresponds to a 180-Vrms excitation of the piezoelectric bender at 5/rev (150 Hz). The volt-ampere apparent power rating for this extreme condition is 43.48 W (0.96% of predicted main rotor steady power consumption at 1800 rpm and 6-deg collective).

VI. Conclusions

This paper presented the development and testing of a four-bladed smart rotor model featuring piezoelectric-bender-actuated trailing-edge flaps for active vibration control. The trailing-edge flap was selected with an 8% span and 20% chord and was located at 75% rotor radius, with associated flap-deflection requirements of ±4 deg for over 95% reduction in the vibratory hub loads. Based on these requirements, an eight-layered tapered actuator excited with a modified input waveform (ac bias circuit) was developed to deflect the 8% span, 20% chord flap by the required deflection amplitude of ±4 deg at the operating speed of 1800 rpm. The rotor blades were developed such that the first torsion frequency was placed close to 3/rev and the third flat-wise bending frequency was placed close to 5/rev. The goal was to maximize actuator control authority in the 3–5/rev frequency range because for a four-bladed rotor the frequencies of interest for vibration suppression are 3, 4, and 5/rev.

The active rotor model was tested in the open-loop mode in hover. These tests showed that the eight-layered actuator had sufficient control authority to meet the ±4-deg requirement. The tests also showed that collective pitch had small influence on actuator performance. This implies that blade steady loads and vehicle trim settings do not affect the actuator-flap control authority. The voltage sweep tests showed that the flap-deflection response exhibited a nonlinear dependence on the actuation voltage. The frequency sweep tests showed that the placement of blade structural flap and torsion natural frequencies was the most dominant design parameter that governs the actuator-flap control authority. This has very important implications for active rotor-blade design optimisation. Purely from a vibration suppression perspective, it is advantageous to place the rotor flat-wise bending and torsion frequencies close to the N/rev, $N-1$/rev, and $N+1$/rev harmonics (where N is the number of blades). The disadvantage of this approach is that it could increase the background vibratory loads and blade dynamic stress levels, potentially leading to reduced fatigue life of the main rotor blades. Therefore design of an active rotor system involves a compromise between maximizing the vibration suppression capability of the actuator flap and maintaining the background vibratory loads and dynamic blade loads within acceptable limits.

The hover tests showed that oscillatory rotor thrust levels of ±10 lb (45 N) (over 60% of steady thrust per blade at 1800 rpm and 6-deg collective) can be generated by the actuation system for 3/rev actuator excitation. This demonstrates the open-loop control effectiveness of the actuation system. However, it has to be noted that the control effectiveness is highly frequency dependent, and this means that careful tailoring of the blade structural frequency placement is necessary for maximizing the actuator authority at the frequencies of interest. Having established the open-loop control

authority of the actuator flap, future work will focus on a full four-bladed closed-loop vibration suppression test to be conducted in the Glenn L. Martin wind tunnel at the University of Maryland.

Acknowledgments

This research was funded by the U.S. Army Research Office under Grant DAAH-04-96-10334 with Gary Anderson serving as the Technical Monitor.

References

[1]Jacklin, A., Nguyen, K., Blaas, A., and Richter, P., "Full-Scale Wind Tunnel Test of a Helicopter Individual Blade Control System," *50th American Helicopter Society Forum*, American Helicopter Society, Alexandria, VA, 1994, pp. 579–596.

[2]Richter, P., Eisbrecher, D., and Kloppel, V., "Design and First Flight Tests of Individual Blade Control Actuators," 16th European Rotorcraft Forum, Sept. 1990.

[3]Straub, F., and Merkley, D., "Design of a Servo-Flap Rotor for Reduced Control Loads," *Journal of Smart Materials and Structures*, Vol. 5, No. 1, 1996, pp. 68–75.

[4]Koratkar, N. A., and Chopra, I., "Analysis and Testing of a Froude-Scaled Rotor with Piezolectric Bender Actuated Trailing-Edge Flaps," *Journal of Intelligent Material Systems and Structures*, Vol. 8, No. 7, 1997, pp. 555–570.

[5]Fulton, M. V., and Ormiston, R. A., "Hover Testing of a Small-Scale Rotor with On-Blade Elevons," *Proceedings of the 53rd Forum of the American Helicopter Society*, American Helicopter Society, Alexandria, VA, 1997.

[6]Prechtl, E. F., and Hall, S. R., "Design of a High Efficiency Discrete Servo-Flap Actuator for Helicopter Rotor Control," Society of Photo-Optical Instrumentation Engineers, Bellingham, WA, March 1997.

[7]Lee, T., and Chopra, I., "Design and Spin Testing of an Active Trailing-Edge Flap Actuated with Piezo-Stacks," 40th Structures, Structural Dynamics, and Materials Conf., April 1999.

[8]Centrolonza, L., and Smith, E., "Design and Experimental Testing of an Induced-Shear Piezoelectric Actuator for Rotor Blade Trailing-Edge Flaps," *Proceedings of the 41st AIAA/ASME/ASCE/AHS/ASC Structures, Structural Dynamics, and Materials Conference*, AIAA, Reston, VA, 2000, pp. 2857–2869.

[9]Fink, D., "Hover Test Featuring Electromagnetic Actuator for Vibration and Acoustic Control," American Helicopter Society, Oct. 2000.

[10]Bernhard, A., and Chopra, I., "Hover Testing of an Active Rotor Blade Tip," *Journal of Intelligent Material Systems and Structures*, Vol. 9, No. 12, 1998, pp. 963–974.

[11]Chen, P. C., and Chopra, I., "Development of a Smart Rotor Blade with Induced Strain Actuation of Blade Twist," *AIAA Journal*, Vol. 35, No. 1, 1997, pp. 6–11.

[12]Rodgers, J. P., and Hagood, N. W., "Design and Manufacture of an Integral-Twist Actuated Rotor Blade," AIAA/ASME/ASCE/AHS/ASC 38th Structures, Structural Dynamics, and Materials Conf., April 1997.

[13]Wilbur, M., Wilkie, W., Yeager, W., Lake, R., Langston, C., Shin, S., and Cesnick, C., "Hover Testing of the NASA/ARL/MIT Active Twist Rotor," 8th Army Research Office Workshop on the Aeroelasticity of Rotorcraft Systems, Oct. 1999.

[14]Koratkar, N. A., and Chopra, I., "Wind Tunnel Testing of a Mach-Scaled Rotor Model with Trailing-Edge Flaps," *Journal of Smart Materials and Structures*, Vol. 10, No. 1, 2001, pp. 1–14.

[15]Koratkar, N. A., and Chopra, I., "Analysis and Testing of Mach-Scaled Rotor with Trailing-Edge Flaps," *AIAA Journal*, Vol. 38, No. 7, 2000, pp. 1113–1124.

[16]"Product Data Sheet," Boca Bearings, Boca Raton, FL, March 1998.

[17]"Design and Fabrication of a Small-Scale Model of 412 Rotor System: Final Design Report," Bell Helicopter Textron, prepared under Contract NAS2-11090, Dec. 1986.

[18]"Siglab 20-42," DSP Technologies, Inc., Freemont, CA, Jan. 1999.

[19]"Model PA9810, Amplifier Technical Manual," Rohrer Systemtechnik, Munich, Aug. 1999.

[20]Sirohi, J., and Chopra, I., "Fundamental Behaviour of Piezoceramic Sheet Actuators," Society of Photo-Optical Instrumentation Engineers, Bellingham, WA, March 1997.

[21]"UM: Calibration Report for Rotor Rig Six-Component Balance," Modern Machine and Tool Inc., Newport News, VA, Jan. 1990.

E. Livne
Associate Editor